Analysis of the Static and Dynamic Stability Properties of the Unmaned Airship

Hae Chang Lee*
Airship Research Department, Aircraft Division
Korea Aerospace Research Institute, Daejeon, Korea 305-600

Abstract

The purpose of this paper is to analyze the static and dynamic stability of the unmanned airship under development ; the target airship's over-all length of hull is 50m and the maximum diameter is 12.5m. For the analysis, the dynamic model of an airship was defined and both the nonlinear and linear dynamic equations of motion were derived. Two different configuration models (KA002Y and KA003Y) of the airship were used for the target model of the static stability analysis and the dynamic stability analysis. From the result of analyses, though the airship is unstable in static stability, dynamic characteristics of the airship can provide the stable dynamic stability. All of the results, airship models and dynamic flight equations will be an important basement and basic information for the next step of developing the automatic flight control system(AFCS) and the stability augmentation system(SAS) for the unmanned airship as well as for the stratospheric airship in the future.

Key Word : flight dynamics, equations of motion of airship, static stability, dynamic stability

Introduction

In the history of world aviation the airship occupied one of the unique milestones of mankind's dream of flying through the sky. It is widely that the airship was the first means of transcontinental air travel , when in the 1920s and 1930s the German Zeppelins provided safe and regular trans-Atlantic crossings between Europe and North and South America. Until the spectacular accident of Hindenburg in 1936 the airship had been successfully operated and culminated in its zenith.

In recent times, interest in the airship arose again, and therefore airship is considered as a new means for conducting multi-roles in civil as well as military applications : for heavy cargo transportation and stratospheric station for multi-purposes. Definitely the advanced technologies can make it possible to be realized : modern envelope materials improve aerodynamic cleanness combined with adequate stiffness, and light weight and modern mechanism for control and propulsion systems also provides more stable and reliable flight characteristics for operating the airship. Korea Aerospace Research Institute (KARI) has launched the development project for stratospheric airship : hull length is about 200m and the first stage is to develop the 50m unmanned non-rigid airship for the prototype to evaluate the automatic flight control system (AFCS) and new concept of propulsion system.

The most important step before applying the AFCS is to define the airship model and flight dynamics equations and to analyze its basic stability characteristics. Though the flight

* Senior Researcher
E-mail : hclee@kari.re.kr. TEL : 042-860-2343. FAX : 042-860-2006

characteristics is similar to that of a fixed-wing airplane, the whole research cumulative works are not matured with respect to the maturity which airplane flight dynamics reached. The airship has many unique and additional features, such as buoyancy, virtual mass, virtual inertia, and so on, which are commonly neglected in airplane analysis.

One purpose of this paper is to briefly review the characteristics of airship's motion and present the analytical model based on some assumptions. Another purpose of this paper is to investigate the static and dynamic stability of two prototype designs of KARI unmanned airship corresponding to the general stability modes of the airship dynamics as the commonly-encountered airplane stability modes, e.g., "Phugoid mode", "Short-Period mode", "Spiral mode", "Dutch-Roll mode", and so on.

Static Stability Analysis

Configuration of Target Airship

The non-rigid type airship configuration studied in this paper has been designed by KARI and has a traditional finned-axisymmetric hull with lift due primarily to buoyancy. The overall length of the hull is 50m, maximum diameter 12.5m, and a fitness ratio 4.0. The helium is used for inflating the envelope where total volume is about 4,090m^3 and inverted-Y type tail fins are attached at the rear of the hull. The propulsion system consists of a gas turbine engine, generator, 2 propellers which are installed at electric motor with a tilting system. Figure 1. shows the configuration of the KARI unmanned airship.

For the convenience, the nomination KA002Y and KA003Y is designated the different configurations and the main difference is that KA002Y's aspect ratio (AR=1.7) of tail fins is greater than KA003Y (AR=1.5) and the leading edge sweepback angle became greater as the design process was going on : from 30° to 40° . These two configurations are the models for analyzing the static and dynamic stability.

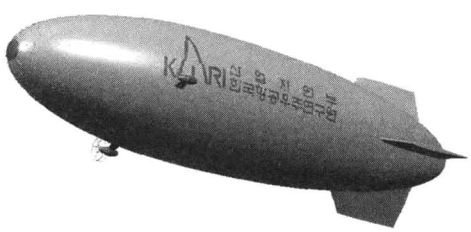

Fig. 1. Configuration of KARI unmanned airship

Table 1. Configuration and performance data

Dimensions				
Type	Non-rigid			
Design c.g	FS:23.5m	BL:0.0m	WL:-300m	
Design c.v	FS:23.925m	BL:0.0m	WL: 0.0m	
Design c.b	FS:23.993m	BL:0.0m	WL: 2.11m (60% inflation ratio)	
Envelope	Length	50.0m	Max. Diameter	12.5m
	Fitness ratio	4.0	Volume	4,090m^3
Tail Fin (3 for each)	LE Sweepback angle	40°	Exposed wetted area	28.434m^2
	Exposed proj. area	27.892m^2	Airfoil section	NACA0006
Performance				
Velocity	Operation	15m/s	Max.	22m/s
Weight	Empty weight	2,400kg	Payload	100kg
Power	< 2kWatt (for equipments)			
Endurance	time	5hours	max. height	5km

Static Stability

The static stability of the airship can be analyzed by investigating the aerodynamic parameters : C_{m_α} and C_{n_β}. Supposing that the airship is flying at the trim point, the static restoring moment can be derived with respect to the center of gravity (c.g.) as Eq. (1). [1]

$$\sum M = M_{CG} = M_{CB} + M_H + M_F + M_T \tag{1}$$

where , M_{CB} is a restoring pitching moment due to buoyancy, M_H due to hull, M_F due to horizontal tail fin and M_T due to thrust. Assuming that the flight path angle (γ) is zero and M_T is so small that it can be neglected, Eq. (1) can be used to derive the non-dimensional derivatives, C_m through dividing it by $q \cdot S_{ref} \cdot l_{ref}$ (q : dynamic pressure, S_{ref} : reference area, l_{ref} : reference length). The reference area is usually selected as $Q^{2/3}$, and the reference length with $Q^{1/3}$ at airship analysis (Q stands for the volume of envelope) [1]. Each contribution to the pitching moment can be obtained with aid of Fig. 2.

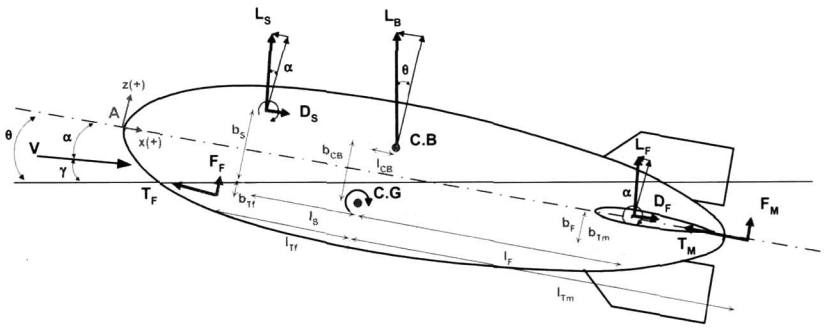

Fig. 2. Static moment equilibrium condition

- Buoyancy contribution : $$(C_m)_{CB} = [(C_L)_{CB} \cdot \cos(\gamma+\alpha)] \cdot \frac{l_{CB}}{l} + [(C_L)_{CB} \cdot \sin(\gamma+\alpha)] \cdot \frac{b_{CB}}{l} \quad (2)$$
- Hull contribution : $$(C_m)_H = [(C_L)_H \cdot \cos\alpha + (C_D)_H \cdot \sin\alpha] \cdot \frac{l_S}{l_{ref}} + [(C_L)_H \cdot \sin\alpha - (C_D)_H \cdot \cos\alpha] \cdot \frac{b_S}{l_{ref}} + (C_{m_\infty})_H \quad (3)$$
- Horizontal tail contribution : $$(C_m)_F = [[(C_L)_h]_{ac} \cdot \cos\alpha + [(C_D)_h]_{ac} \cdot \sin\alpha] \cdot \eta_F \cdot (V_H)_{lf} + [[(C_L)_h]_{ac} \cdot \sin\alpha - [(C_D)_h]_{ac} \cdot \cos\alpha] \cdot \eta_F \cdot (V_H)_{bf} + (C_{m_\infty})_F \quad (4)$$

where S_F stands for the area of horizontal tail, and tail efficiency factor (η_F) and tail volume coefficient (V_H) can be defined as follows :

$$\eta_F = \frac{q_F}{q}, \qquad (V_H)_{lf} = \left(\frac{S_F \cdot l_F}{S_{ref} \cdot l_{ref}}\right), \qquad (V_H)_{bf} = \left(\frac{S_F \cdot b_F}{S_{ref} \cdot l_{ref}}\right)$$

The pitching moment coefficient can be obtained from the lift and drag results computed by CFD (Computational Fluid Dynamics). These results are summarized in Table 1, Fig. 3, Fig. 4, and Fig. 5, and are also compared with the wind tunnel test data of the U.S. airship, AKRON, which was operated in 1920s by U.S. Navy [2].

Table 1. Lift, drag and pitching moment (Longitudinal)

aoa(α)	C_L			C_D			C_M		
	AKRON	KA003Y	KA002Y	AKRON	KA003Y	KA002Y	AKRON	KA003Y	KA002Y
-3°	-0.030	-0.047	-0.047	0.026	0.034	0.034	-0.036	-0.032	-0.0322
0°	0.004	0.0	0.0	0.025	0.032	0.032	0.004	-0.0002	-0.0002
3°	0.037	0.046	0.046	0.028	0.034	0.034	0.050	0.0329	0.033
6°	0.079	0.102	0.101	0.032	0.039	0.039	0.082	0.0568	0.0579
9°	0.132	0.166	0.163	0.044	0.051	0.050	0.098	0.0717	0.0748
12°	0.199	0.237	0.232	0.062	0.070	0.068	0.100	0.0781	0.0842
15°	0.274	0.313	0.304	0.091	0.098	0.095	0.084	0.0765	0.0867
18°	0.356	0.392	0.380	0.131	0.137	0.130	0.059	0.0673	0.0828
20°	0.414	0.442	0.428	0.160	0.166	0.157	0.039	0.0617	0.0795

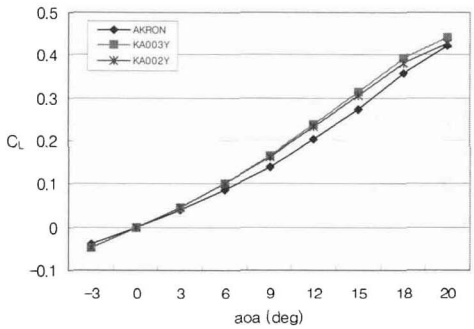

Fig. 3. Lift curve of airship

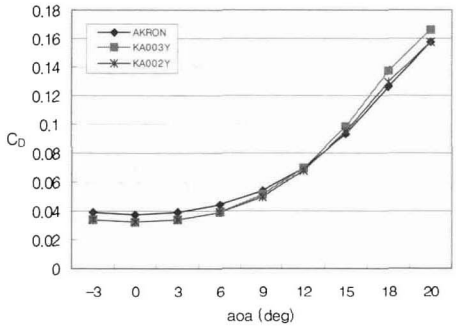

Fig. 4. Drag curve of airship

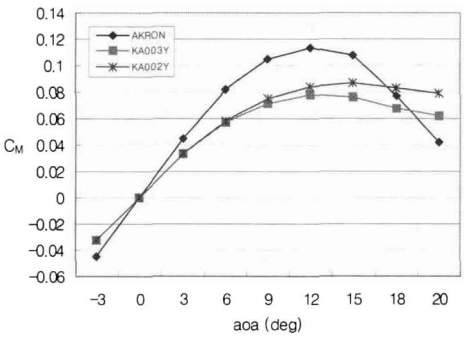

Fig. 5. Lift curve of airship

The slopes of the pitching moment curve given in Fig. 5 indicate that airship is unstable for the angle of attack up to around 12° ($C_{m_\alpha} > 0$), is then approximately neutrally stable for a small range, and is stable for pitch angles greater than 12° . The instability of KA002Y and KA003Y is somewhat less than that of AKRON. This typical feature of airship is one of the major different properties as compared with the one of conventional airplane. Though it seems to contradict the fact that the airship is more stable than the airplane, the airship can provide the stability in the view point of the dynamic behavior : the large part of the airship hull can yield the great damping effects when it maneuvers with angular rate [3]. Considering the lift and drag coefficients from Fig. 3 and Fig.4, the difference is very small for the three airship models.

Flight Dynamic Model of the Airship

Equations of Motion

The mathematical descriptions of the dynamic stability analysis are derived from the linearized equations of motion of the airship. For the purposes of modeling the flight dynamics of the airship, we made assumptions similar to those for aircraft ; the vehicle is assumed to be perfectly rigid body and flying at a mean reference flight speed. However the center of volume (c.v), not the center of gravity (c.g), is chosen as the origin of the airship body axis, as shown in Fig. 6 [5]. The buoyancy force (B), virtual mass, and inertia terms are significant in addition to the familiar aircraft equations of motion. The virtual mass and virtual inertia effects arise due to the airship's mass being of the same order of magnitude as the mass of displaced air, and are described as force and moment with respect to the linear and angular accelerations in Eq. (5) and (6) [1].

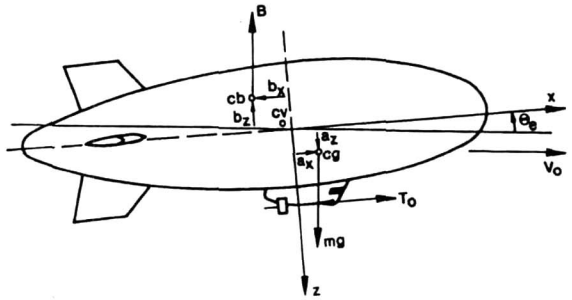

Fig. 6. General airship reference system

- Virtual mass : $m_x = m - X_{\dot{u}}$, $m_y = m - Y_{\dot{v}}$, $m_z = m - Z_{\dot{w}}$ (5)
- Virtual inertia : $J_x = I_x - L_{\dot{p}}$, $J_y = I_y - M_{\dot{q}}$, $J_z = I_z - N_{\dot{r}}$ (6)

$$J_{xy} = I_{xy} + L_{\dot{q}} \equiv I_{xy} + M_{\dot{p}}, \quad J_{xz} = I_{xz} + N_{\dot{p}} \equiv I_{xz} + L_{\dot{r}}, \quad J_{yz} = I_{yz} + M_{\dot{r}} \equiv I_{yz} + N_{\dot{q}}$$

where m is the mass of the airship, X, Y, Z is the external force, L, M, N is the external moment of the body axis, respectively, and the conventional notation is the same as the aircraft' aerodynamic dimensional derivatives : $X_{\dot{u}} \equiv \frac{\partial X}{\partial \dot{u}}$.

The rigid body equations of motion are obtained using Newton's second law. The velocity, $\vec{V}$, is slightly different from the one of the aircraft because the point of c.g is not coincide with the origin of body axis and is described as Eq. (8) [6].

$$\vec{F} = \frac{d(m\vec{V})}{dt}, \qquad \vec{M} = \frac{d\vec{H}}{dt} \tag{7}$$

$$\vec{V} = \vec{\mu} + \frac{d\vec{\rho}}{dt} = \vec{\mu} + \vec{\omega} \times \vec{\rho} \tag{8}$$

where $\vec{\mu}$ is the velocity vector of the body axis, $\vec{\rho}$ is the displacement vector from the origin of body axis to the c.g, and $\vec{\omega}$ stands for the angular rate vector. Each vector can be defined as Eq. (9) by using the unit vector of body axis as $\vec{i}_b$, $\vec{j}_b$, $\vec{k}_b$.

$$\vec{\mu} = U\,\vec{i}_b + V\,\vec{j}_b + W\,\vec{k}_b, \quad \vec{\rho} = x\,\vec{i}_b + y\,\vec{j}_b + z\,\vec{k}_b, \quad \vec{\omega} = P\,\vec{i}_b + Q\,\vec{j}_b + R\,\vec{k}_b \tag{9}$$

Substituting Eqs. (5), (6), (8) and (9) into Eq. (7) yields the following equations.

$$\begin{aligned}\vec{F} = {} & \left[m_x\dot{U} + m_zQW - m_yRV + (ma_z - X_{\dot{q}})\dot{Q} - (ma_y + X_{\dot{r}})\dot{R} - ma_x(Q^2 + R^2) + ma_yPQ - ma_zPR\right]\vec{i}_b \\ & + \left[m_y\dot{V} - m_zPW + m_xRU - (ma_z + Y_{\dot{p}})\dot{P} + (ma_x - Y_{\dot{r}})\dot{R} - ma_y(P^2 + R^2) + ma_xPQ + ma_zQR\right]\vec{j}_b \\ & + \left[m_z\dot{W} + m_yPV - m_xQU + (ma_y - Z_{\dot{p}})\dot{P} - (ma_x + Z_{\dot{q}})\dot{Q} - ma_z(P^2 + Q^2) + ma_xPR + ma_yQR\right]\vec{k}_b\end{aligned} \tag{11}$$

$$\begin{aligned}\vec{M} = {} & \left[J_x\dot{P} - J_{xy}(\dot{Q} - PR) - J_{xz}(\dot{R} + PQ) + J_{yz}(R^2 - Q^2) + (J_z - J_y)QR + ma_y(\dot{W} + PV - QV) - ma_z(\dot{V} + RU - PW)\right]\vec{i}_b \\ & + \left[-J_{xy}(\dot{P} + QR) + J_y\dot{Q} - J_{yz}(\dot{R} - PQ) + J_{xz}(P^2 - R^2) + (J_x - J_z)PR - ma_x(\dot{W} + PV - QU) + ma_z(\dot{U} + QW - RV)\right]\vec{j}_b \\ & + \left[-J_{xz}(\dot{P} - QR) - J_{yz}(\dot{Q} + PR) + J_z\dot{R} + J_{xy}(Q^2 - P^2) + (J_y - J_x)PQ + ma_x(\dot{V} + RU - PW) - ma_y(\dot{U} + QW - RV)\right]\vec{k}_b\end{aligned}$$

Since the airship is symmetric about the oxz plane, $J_{xy} = J_{yz} = 0,\ a_y = 0$. Then the six degree of freedom equations of motion can be developed, and terms of the right hand side of the Eqs. (12) and (13) are composed of aerodynamic force and moment, gravitational force, buoyancy and propulsive force, respectively.

- Axial Force : $m_x\dot{U} + m_zQW - m_yRV + (ma_z - X_{\dot{q}})\dot{Q} - ma_x(Q^2 + R^2) - ma_zPR = X$
- Side Force : $m_y\dot{V} - m_zPW + m_xRU - (ma_z + Y_{\dot{p}})\dot{P} + (ma_x - Y_{\dot{r}})\dot{R} + ma_xPQ + ma_zQR = Y$ (12)
- Normal Force : $m_z\dot{W} + m_yPV - m_xQU - (ma_x + Z_{\dot{q}})\dot{Q} - ma_z(P^2 + Q^2) + ma_xPR = Z$

- o Rolling Moment : $J_x\dot{P} - J_{xz}(\dot{R} + PQ) + (J_z - J_y)QR - (ma_z + L_{\dot{v}})\dot{V} - ma_z(\dot{V} + RU - PW) = L$
- o Pitching Moment : $J_y\dot{Q} + J_{xz}(P^2 - R^2) + (J_x - J_z)PR - (ma_x + M_{\dot{w}})\dot{W}$
  $- ma_x(PV - QU) + (ma_z - M_{\dot{u}})\dot{U} + ma_z(QW - RV) = M$ (13)
- o Yawing Moment : $J_z\dot{R} - J_{xz}(\dot{P} - QR) + (J_y - J_x)PQ + (ma_x - N_{\dot{v}})\dot{V} + ma_x(RU - PW) = N$

Linearized Longitudinal Dynamic Equations

The equations developed in the previous section can be linearized by using the small perturbation theory about the trimmed equilibrium flight condition. By introducing the small perturbation variables such as u, v, w and p, q, r (velocity and angular rate), Eqs. (12) and (13) can be simplified and decoupled [7].

The linearized longitudinal equations can therefore be written from Eq. (12) and (13) as follows.

$$
\begin{aligned}
&m_x\dot{u} + (ma_z - X_{\dot{q}})\dot{q} = X_u u + X_w w + (X_q - m_zW_e)q + X_{\delta e}\delta_e + X_t\delta_t - (mg - B)\theta\cdot\cos\theta_e \\
&m_z\dot{w} - (ma_x + Z_{\dot{q}})\dot{q} = Z_u u + Z_w w + (Z_q + m_xU_e)q + Z_{\delta e}\delta_e + (mg - B)\theta\cdot\sin\theta_e \\
&J_y\dot{q} + (ma_z - M_{\dot{u}})\dot{u} - (ma_x - M_{\dot{w}})\dot{w} = M_u u + M_w w + (M_q - ma_xU_e - ma_zW_e)q + M_t\delta_t + M_{\delta e}\delta_e \\
&\qquad\qquad - \theta\{(mga_z + Bb_z)\cos\theta_e\} - (mga_z + Bb_z)\sin\theta_e
\end{aligned}
\tag{14}
$$

where $U_e, W_e, T_e, X_e, \theta_e$ denote the values at trimmed state, θ is the pitch angle, T is the thrust and δ_e and δ_t are for the elevator and throttle deflection, respectively. Simplifying the above presentation of equations of motion in the state space form, Eq. (14) can be represented.

$$\mathbf{m}\cdot\dot{\mathbf{x}} = \mathbf{a}\cdot\mathbf{x} + \mathbf{b}\cdot\mathbf{u} \tag{15}$$

where

$$\mathbf{x}^T = [u \quad w \quad q \quad \theta] \qquad \mathbf{u}^T = [\delta_e \quad \delta_t]$$

$$
\mathbf{m} = \begin{bmatrix} m_x & 0 & (ma_z - X_{\dot{q}}) & 0 \\ 0 & m_z & -(ma_x + Z_{\dot{q}}) & 0 \\ (ma_z - M_{\dot{u}}) & -(ma_x + M_{\dot{w}}) & J_y & 0 \\ 0 & 0 & 0 & 1 \end{bmatrix}
$$

$$
\mathbf{a} = \begin{bmatrix} X_u & X_w & (X_q - m_zW_e) & -(mg - B)\cdot\cos\theta_e \\ Z_u & Z_w & (Z_q + m_xU_e) & -(mg - B)\cdot\sin\theta_e \\ M_u & M_w & (M_q - ma_xU_e - ma_zW_e) & -\{(mga_z + Bb_z)\cdot\cos\theta_e - (mga_x + Bb_x)\cdot\sin\theta_e\} \\ 0 & 0 & 1 & 0 \end{bmatrix}
\qquad
\mathbf{b} = \begin{bmatrix} X_{\delta e} & X_t \\ Z_{\delta e} & 0 \\ M_{\delta e} & M_t \\ 0 & 0 \end{bmatrix}
\tag{16}
$$

Multiplying the inverse matrix, $\mathbf{m}^{-1}$, in the both sides can reduce Eqs. (15) and (16) to the typical state space representation.

$$\dot{\mathbf{x}} = \mathbf{m}^{-1} \cdot \mathbf{a} \cdot \mathbf{x} + \mathbf{m}^{-1} \cdot \mathbf{b} \cdot \mathbf{u} = \mathbf{A} \cdot \mathbf{x} + \mathbf{B} \cdot \mathbf{u} \tag{17}$$

$$\mathbf{A} = \begin{bmatrix} x_u & x_w & x_q & -(mg - B)\cdot\cos\theta_e \\ z_u & z_w & z_q & -(mg - B)\cdot\sin\theta_e \\ m_u & m_w & m_w & -\{(mga_z + Bb_z)\cdot\cos\theta_e - (mga_x + Bb_x)\cdot\sin\theta_e\} \\ 0 & 0 & 1 & 0 \end{bmatrix} \quad \mathbf{B} = \begin{bmatrix} x_{\delta e} & x_t \\ z_{\delta e} & 0 \\ m_{\delta e} & m_t \\ 0 & 0 \end{bmatrix} \tag{18}$$

Linearized Lateral-Directional Dynamic Equations

The linearized lateral-directional equations of motion can be also derived.

$$\begin{aligned} m_y\dot{v} - (ma_z + Y_{\dot{p}})\dot{p} + (ma_x - Y_{\dot{r}}) &= Y_v v + (Y_p + m_z W_e)p + (Y_r - m_x U_e)r + Y_{\delta r}\delta_r + (mg - B)\phi\cdot\cos\theta_e \\ J_x\dot{p} - J_{xz}\dot{r} - (ma_z + L_{\dot{v}})\dot{v} &= L_v v + (L_p - ma_z W_e)p + (L_r + ma_z U_e)r - (mga_z + Bb_z)\phi\cdot\cos\theta_e \\ J_z\dot{r} - J_{xz}\dot{p} + (ma_x - N_{\dot{v}})\dot{v} &= N_v v + (N_p + ma_x W_e)p + (N_r - ma_x U_e)r + N_{\delta r}\delta_r + (mga_x + Bb_x)\phi\cdot\cos\theta_e \end{aligned} \tag{19}$$

where ϕ is the roll angle and δ_r is the rudder deflection. Same as the linearized longitudinal equations, Eq. (19) can be simplified as the form of Eq. (15).

$$\mathbf{x}^T = [v \quad p \quad r \quad \phi] \qquad \mathbf{u}^T = [\delta_r]$$

$$\mathbf{m} = \begin{bmatrix} m_y & -(ma_z + Y_{\dot{p}}) & (ma_x - Y_{\dot{r}}) & 0 \\ -(ma_z + L_{\dot{v}}) & J_x & -J_{xz} & 0 \\ (ma_z - N_{\dot{v}}) & -J_{xz} & J_z & 0 \\ 0 & 0 & 0 & 1 \end{bmatrix}$$

$$\mathbf{a} = \begin{bmatrix} Y_v & (Y_p + m_z W_e) & (Y_r - m_x U_e) & (mg - B)\cdot\cos\theta_e \\ L_v & (L_p - ma_z W_e) & (L_r + ma_z U_e) & -(mga_z + Bb_z)\cdot\cos\theta_e \\ N_v & (N_p + ma_x W_e) & (N_r - ma_x U_e) & (mga_x + Bb_x)\cdot\cos\theta_e \\ 0 & 1 & 0 & 0 \end{bmatrix} \quad \mathbf{b} = \begin{bmatrix} Y_{\delta r} \\ 0 \\ N_{\delta r} \\ 0 \end{bmatrix} \tag{20}$$

Again, multiplying the inverse matrix, $\mathbf{m}^{-1}$, in the both sides can reduce Eq. (20) into the state space form of Eq. (17).

$$\mathbf{A} = \begin{bmatrix} y_v & y_p & y_r & (mg - B)\cdot\cos\theta_e \\ l_v & l_p & l_r & -(mga_z + Bb_z)\cdot\cos\theta_e \\ n_v & n_p & n_r & (mga_x + Bb_x)\cdot\cos\theta_e \\ 0 & 1 & 0 & 0 \end{bmatrix} \quad \mathbf{B} = \begin{bmatrix} y_{\delta r} \\ 0 \\ n_{\delta r} \\ 0 \end{bmatrix} \tag{21}$$

Equations (18) and (21) consist of the dimensional aerodynamic derivatives and these should be calculated using the non-dimensional derivatives through some methods. In this paper, all aerodynamic derivatives were calculated from the results of CFD calculations for two models of airship, KA002Y and KA003Y.

Dynamic Stability Analysis

The dynamic stability can be analyzed by investigating the eigenvalues (λ_r) of the system matrix **A** in Eqs. (18) and (21). For a nontrivial solution to exist, the determinant must be zero [8].

$$|\lambda \mathbf{I} - \mathbf{A}| = 0$$

The natural frequency(ω_n) and damping coefficient(ζ) of the system are readily obtained once the eigenvalues are computed and consequently the period(P), the time constant(T) and the time to half amplitude($T_{1/2}$) can be defined. For the specific flight conditions, each airship was assumed to fly under the neutral buoyancy condition ($mg-B=0$) and five flight conditions with flight speed 3m/s, 8m/s, 12m/s, 20m/s and 25m/s are considered. The aerodynamic derivatives of KA002Y and KA003Y were calculated in accordance with the flight condition by CFD method and the results of which are summarized in Table 2 [4]. All the results of stability analysis were compared with the characteristics of YAZ-2A of U.S. Navy airship in 1980s [5].

Table 2. Non-dimensional aerodynamic derivatives

	Longitudinal motion						
configuration	C_L	C_D	C_m	C_{L_α}	C_{m_α}	C_{L_q}	C_{m_q}
KA002Y	0.0	0.0291	0.0	0.7907	0.6911	4.1117	-0.1832
KA003Y	0.0	0.0291	0.0	0.8480	0.5543	4.3578	-0.8507

	Lateral-Directional motion								
configuration	C_{y_β}	C_{y_p}	C_{y_r}	C_{l_β}	C_{l_p}	C_{l_r}	C_{n_β}	C_{n_p}	C_{n_r}
KA002Y	-0.7850	0.0007	4.047	0.0006	-0.0998	0.0141	-0.7023	-0.001	-0.0799
KA003Y	-0.8365	0.0007	4.437	0.0002	-0.1189	0.0178	-1.1850	-0.001	-0.8211

Longitudinal Stability

The eigenvalues of the longitudinal dynamic modes of airship have two negative real roots and one complex conjugate pair and these solutions characterize the stability modes of the longitudinal dynamics as three kinds of categories : 1) longitudinal pendulum mode(LPM), 2) surge mode (SM), and 3) heave mode(HM) (or pitch subsidence mode) [5].

Table 3. Results of the longitudinal stability analysis

V	MODE	YAZ-2A					KA002Y					KA003Y				
		λ_r	ω_n (rad/s)	ζ	P or T (sec)	$T_{1/2}$ (sec)	λ_r	ω_n (rad/s)	ζ	P or T (sec)	$T_{1/2}$ (sec)	λ_r	ω_n (rad/s)	ζ	P or T (sec)	$T_{1/2}$ (sec)
25 m/s	SM	-0.0273			36.65	25.29	-0.0807			12.39	8.55	-0.0808			12.38	8.54
	HM	-1.1154			0.90	0.62	-0.1306			7.66	5.28	-0.1121			8.92	6.15
	LPM	-0.0771 ±0.0898i	0.1184	0.6517	70.00	8.94	-0.3489 ±0.8657i	0.9334	0.3738	7.26	1.98	-0.6042 ±0.8481i	1.0413	0.5802	7.41	1.14
20 m/s	SM	-0.0216			46.25	31.91	-0.0643			15.54	10.72	-0.0644			15.54	10.72
	HM	-0.8594			1.16	0.80	-0.1518			6.59	4.55	-0.1357			7.37	5.08
	LPM	-0.0786 ±0.0914i	0.1206	0.6520	68.74	8.78	-0.2555 ±0.7315i	0.7749	0.3298	8.59	2.70	-0.4604 ±0.7114i	0.8474	0.5434	8.83	1.50
12 m/s	SM	-0.0135			73.93	51.01	-0.0386			25.90	17.87	-0.0386			25.90	17.87
	HM	-0.3706			2.70	1.86	-0.1739			5.75	3.97	-0.1758			5.69	3.92
	LPM	-0.1196 ±0.0764i	0.1419	0.8426	82.23	5.77	-0.1119 ±0.5498i	0.5611	0.1995	11.43	6.17	-0.2291 ±0.5296i	0.3970	0.5771	11.86	3.01
8 m/s	SM	-0.0090			110.89	76.51	-0.0257			38.94	26.87	-0.0257			38.94	26.87
	HM	-0.0682			14.66	10.12	-0.1547			6.46	4.46	-0.1650			6.06	4.18
	LPM	-0.1692 ±0.2106i	0.2702	0.6264	29.83	4.08	-0.0552 ±0.4824i	0.4856	0.1138	13.02	12.49	-0.1288 ±0.4690i	0.4863	0.2649	13.40	5.36
3 m/s	SM	-0.0034			293.43	202.47	-0.0096			103.90	71.69	-0.0096			103.90	71.69
	HM	-0.0221			45.30	31.26	-0.0755			13.24	9.13	-0.0810			12.34	8.51
	LPM	-0.0652 ±0.2830i	0.2904	0.2245	22.20	10.58	-0.0120 ±0.4255i	0.4257	0.0281	14.76	57.64	-0.0387 ±0.4232i	0.4249	0.0911	14.85	17.82

Longitudinal pendulum mode is approximately characterized by M_q and M_θ at low speed range and by Z_w, Z_q, M_w, M_q and M_θ at high speed range. This mode dominates the response characteristics of pitch angle and the motion property associated with this mode is a lightly damped oscillation [5]. As speed increases, this oscillatory motion becomes more stable. Figure 7. shows the location of the poles in the upper half side of complex plane. Figure 8. presents the

variation of frequency and damping ratio of LPM , Fig. 9. period variation, and Fig. 10. time to half amplitude variation of the LPM, respectively. The tendency of frequency and damping ratio of KA02Y and KA003Y is to increase as the flight speed does. The period reflects the same properties as shown in Fig. 9. On the contrary, the restoring response of KA003Y is fast rather than that of Ka002Y because the damping ratio is large.

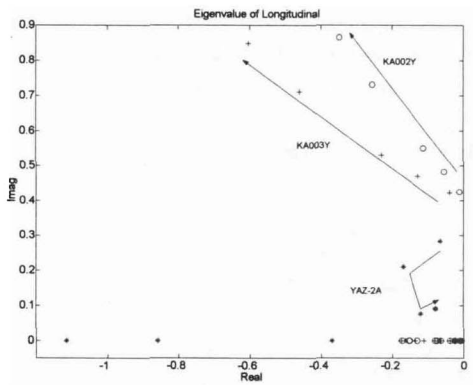

Fig. 7. Eigenvalues of longitudinal stability

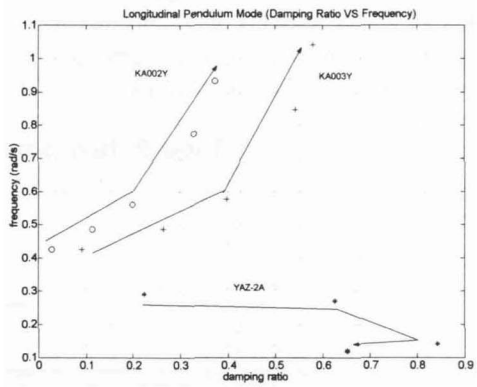

Fig. 8. Frequency vs damping of LPM

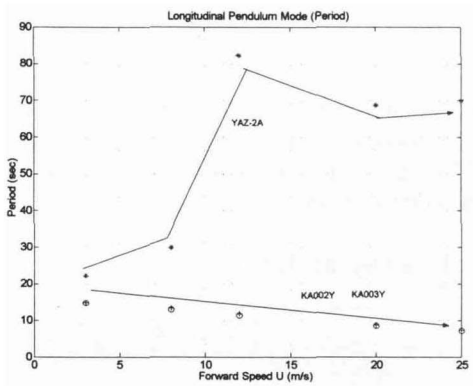

Fig. 9. Period variation of LPM

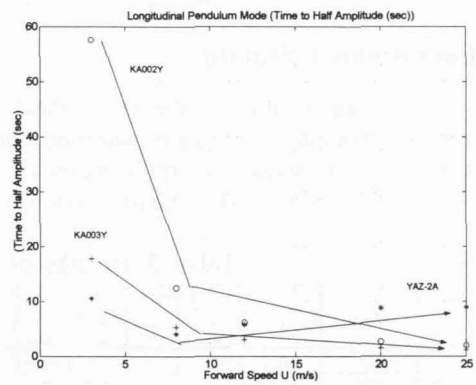

Fig. 10. Time to half amplitude of LPM

The surge mode is the real one whose root is located in the negative imaginary axis and appears as a stable speed subsidence, with approximate time constant $T \cong -1/X_u$, therefore this mode dominates the dynamic characteristics of axial speed, u [1]. The characteristics of the surge mode at all speeds is shown in Fig. 11 and 12.

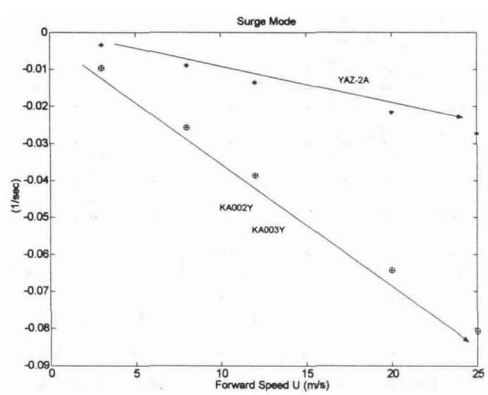

Fig. 11. Eigenvalue variation of SM

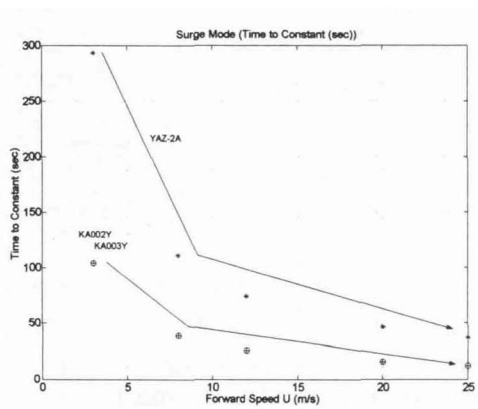

Fig. 12. Time constant of SM

As the speed increases, as shown in Fig. 11, the pole of the surge mode decreases almost linearly with speed, in adverse the aerodynamic damping derivatives decreases almost linearly with speed. The difference between two configurations, KA002Y and KA003Y is very small but the time to constant of two configurations is three times as fast as that of YAZ-2A.

At low speed the heave mode is characterized approximately by Z_w and at high speed it becomes a pitch subsidence mode characterized approximately by M_q. This mode also demonstrated the response of pitch rate. Same as the surge mode, KA002Y and KA003Y's properties would have a little difference and time constant becomes faster at the speed range of 3m/s~12m/s ((13.24 sec → 5.75 sec, KA002Y), however this tendency is adverse at the range of 12m/s~25m/s (5.75 sec → 7.66 sec, KA002Y).

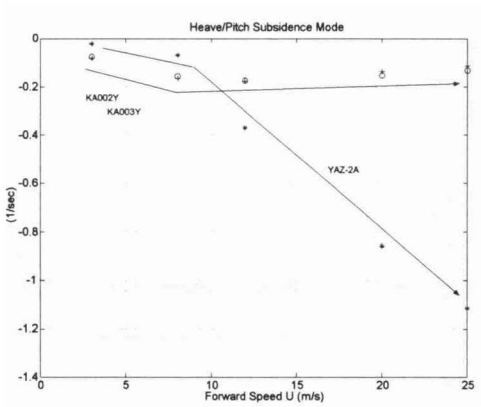

Fig. 13. Eigenvalue variation of HM

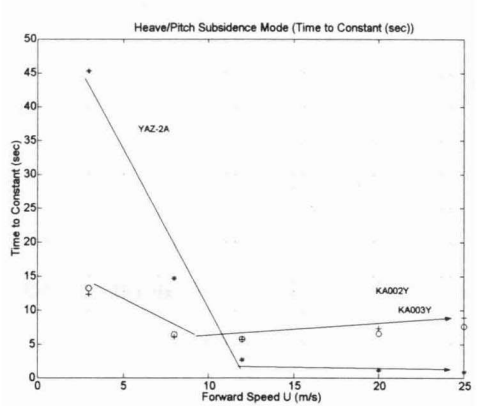

Fig. 14. Time constant of HM

The impulse response of longitudinal motion are shown on the speed, 25m/s and 3m/s in Fig. 15. and 16.

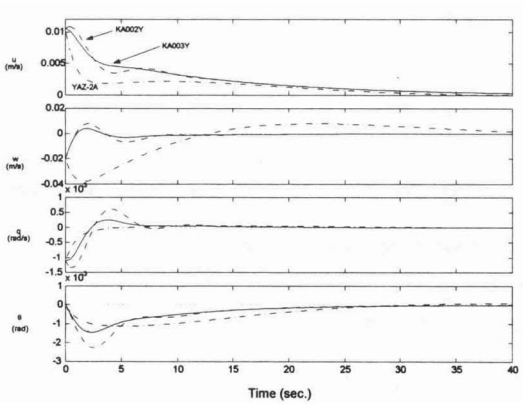

Fig. 15. Impulse response at 25m/s of longitudinal

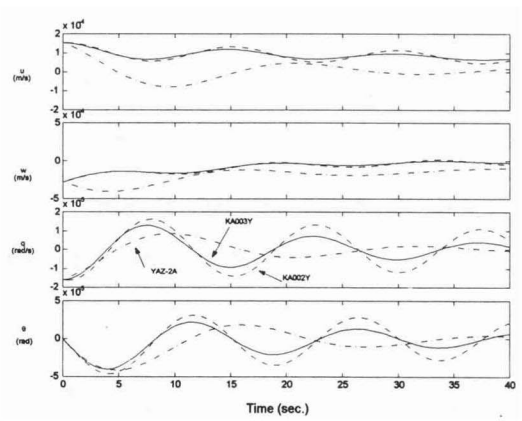

Fig. 16. Impulse response at 3m/s of longitudinal

Lateral-Directional Stability

The eigenvalues of the lateral-directional dynamic of airship have two negative real roots and one complex conjugate pair and these modes characterize the stability modes of the lateral-directional dynamic as three kinds of categories : 1) roll oscillation mode(ROM), 2) sideslip subsidence mode (SSM), and 3) yaw subsidence mode(YSM). The results are summarized in Table 4 [5].

Roll oscillation mode is the first complex conjugate and approximately characterized by L_v, L_p, L_ϕ and Y_ϕ at high speed range and L_ϕ is neglected at low speed, respectively. This mode

dominates the oscillatory motion of roll rate and roll angle, which is dynamically similar to the longitudinal pendulum mode. In KA002Y and KA003Y the frequency and damping ratio is larger than that of YAZ-2A, therefore the period is about two times as fast as that of YAZ-2A (Table 4. and Fig. 18.). The change in frequency with respect to the speed is not so large that the period change in Fig. 19. seems to be constant over the whole speed range ; KA002Y's ω_n : 1.4586 (V=3m/s) ~ 1.6237 (V=25m/s), KA003Y's ω_n : 1.4602 (V=3m/s) ~ 1.9372 (V=25m/s)

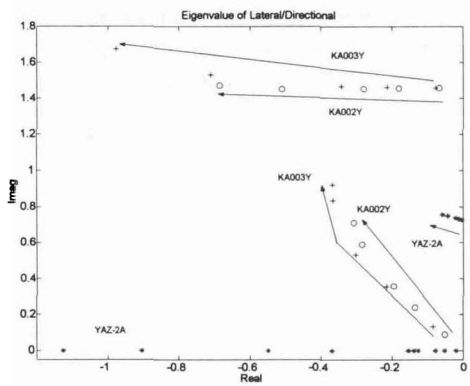

Fig. 17. Eigenvalues of lateral stability

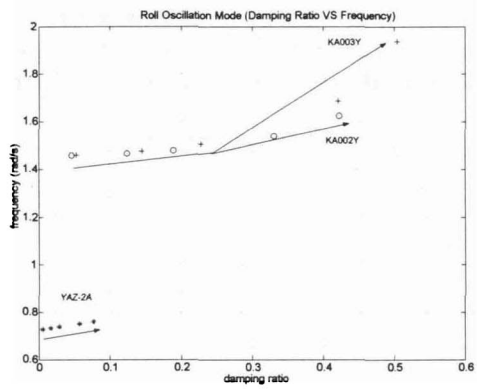

Fig. 18. Frequency vs damping of ROM

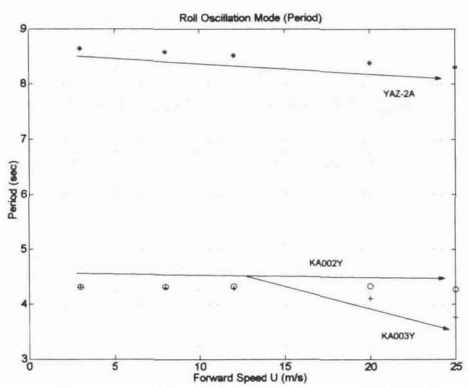

Fig. 19. Period variation of ROM

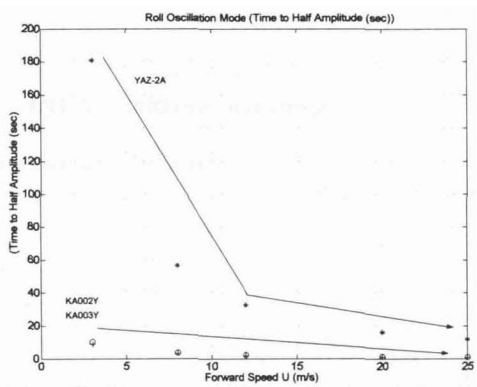

Fig. 20. Time to half amplitude of ROM

Table 4. Results of the lateral-directional stability analysis

V	MODE	YAZ-2A					KA002Y					KA003Y				
		λ_r	ω_n (rad/s)	ζ	P or T (sec)	$T_{1/2}$ (sec)	λ_r	ω_n (rad/s)	ζ	P or T (sec)	$T_{1/2}$ (sec)	λ_r	ω_n (rad/s)	ζ	P or T (sec)	$T_{1/2}$ (sec)
25 m/s	SSM	-0.1551			6.45	4.45	-0.3077 ±0.7124i	0.7761	0.3965	8.82	2.24	-0.3680 ±0.9217i	0.9924	0.3708	6.82	1.88
	YSM	-1.1262			0.89	0.61										
	ROM	-0.0583 ±0.7571i	0.7593	0.0768	8.30	11.83	-0.6852 ±1.4721i	1.6237	0.4220	4.27	1.01	-0.9776 ±1.6725i	1.9372	0.5046	3.76	0.71
20 m/s	SSM	-0.1265			7.90	5.45	-0.2847 ±0.5902i	0.6552	0.4345	10.65	2.42	-0.3667 ±0.8348i	0.9118	0.4022	7.53	1.88
	YSM	-0.9040			1.11	0.76										
	ROM	-0.0429 ±0.7495i	0.7508	0.0572	8.38	16.07	-0.5096 ±1.4520i	1.5388	0.3312	4.33	1.36	-0.7098 ±1.5304i	1.6870	0.4207	4.11	0.97
12 m/s	SSM	-0.0776			12.88	8.89	-0.1966 ±0.3583i	0.4087	0.4810	17.54	3.51	-0.3028 ±0.5327i	0.6128	0.4941	11.79	2.28
	YSM	-0.5484			1.82	1.26										
	ROM	-0.0211 ±0.7379i	0.7382	0.0286	8.52	32.63	-0.2800 ±1.4526i	1.4793	0.1893	4.33	2.46	-0.3431 ±1.4661i	1.5057	0.2279	4.29	2.01
8 m/s	SSM	-0.0522			19.17	13.23	-0.1357 ±0.2395i	0.2753	0.4930	26.23	5.08	-0.2164 ±0.3563i	0.4168	0.5191	17.64	3.20
	YSM	-0.3690			2.71	1.88										
	ROM	-0.0122 ±0.7323i	0.7324	0.0166	8.58	56.61	-0.1820 ±1.4553i	1.4667	0.1241	4.32	3.79	-0.2142 ±1.4612i	1.4768	0.1451	4.30	3.22
3 m/s	SSM	-0.0198			50.40	34.78	-0.0520 ±0.0894i	0.1034	0.5026	70.28	13.27	-0.0845 ±0.1333i	0.1578	0.5352	47.13	8.17
	YSM	-0.1396			7.16	4.94										
	ROM	-0.0038 ±0.7274i	0.0667	0.0052	8.64	180.84	-0.0672 ±1.4573i	1.4589	0.0460	4.31	10.27	-0.0770 ±1.4582i	1.4602	0.0527	4.31	8.96

The sideslip subsidence mode is dominated approximately by the aerodynamic derivatives such as L_v, L_ϕ, Y_v and Y_ϕ and characterizes the response of the y-axis velocity, v. One another real root represents the yaw subsidence mode, which is characterized by the L_v, L_ϕ, Y_v, Y_ϕ, Y_r, N_v, N_ϕ and N_r and is the response of the yaw rate [5]. These two modes are always stable without oscillation.

However unfortunately both of the above two modes would not be present in KA002Y and KA003Y due to the heavy damping effects of some aerodynamic derivatives and the new oscillatory mode would be present and compounded of two modes, sideslip subsidence mode and yaw subsidence mode. This mode is named as lateral mode 1 (LM1) in this study. Though the lateral mode 1 is similar to the roll oscillation mode, it shows faster and more stable dynamics of motion (Fig. 22). In other words, its frequency and damping ratio is greater than that of the roll oscillation mode. In addition the change of the damping ratio is not so large when the flight speed increases : KA002Y's ζ =0.5026 (V=3m/s) ~ 0.3965 (V=25m/s), KA003Y's ζ =0.5352 (V=3m/s) ~ 0.3708 (V=25m/s).

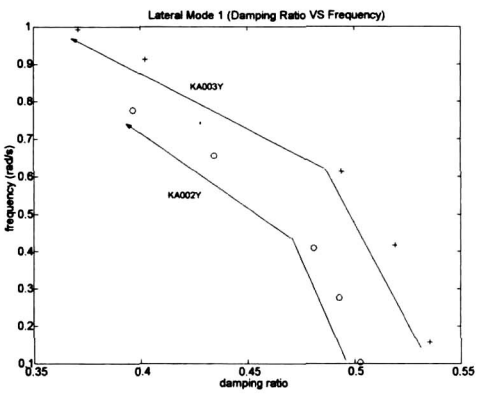

Fig. 21. Frequency vs damping of LM1

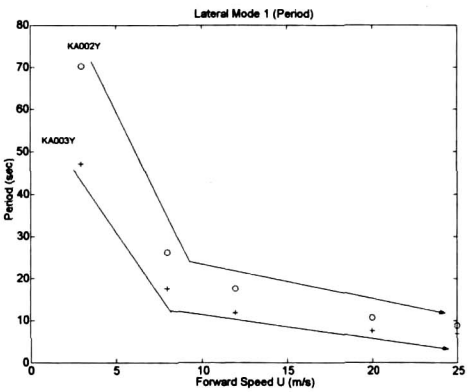

Fig. 22. Period variation of LM1

The impulse responses of lateral-directional motion are shown for the speed, 25m/s and 3m/s in Figs. 23. and 24., respectively. Similar to the characteristics of longitudinal motion, the dynamic characteristic responses of KA003Y and KA002Y are more faster than that of YAZ-2A, but the property of KA002Y's response is less stable than that of KA003Y.

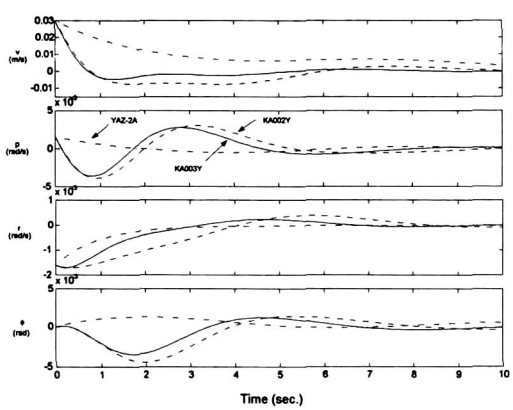

Fig. 23. Impulse response at 25m/s of lateral

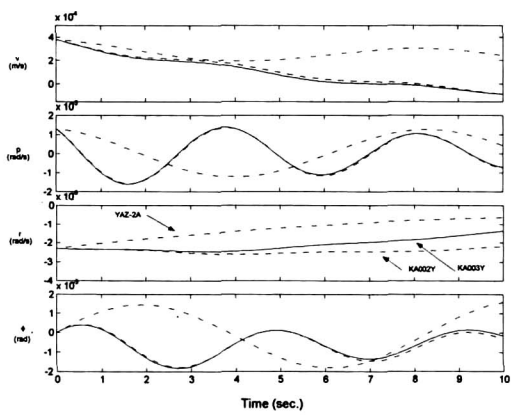

Fig. 24. Impulse response at 3m/s of lateral

Conclusions

The analysis of the static stability was performed in view point of the static moment equilibrium of the longitudinal dynamics for two configurations of KARI unmanned airship. The numerical results has shown that the airship's static stability is unstable in comparison to that of the conventional aircraft.

The dynamic model of the airship was defined and the equations of motion were derived for the dynamic analyses. Those linearized equations of motion can provide the useful framework to analyze the dynamic stability of the airship and all of the results were obtained based on the neutrally buoyant condition. All modes of the airship were analyzed, and some modes of lateral-directional motion were not coincide with the typical airship's stability modes.

The dynamic stability analyses of two configurations shows that all modes are stable at over the entire speed envelope. In addition, the dynamic response of KA003Y is a little faster than that of KA002Y in longitudinal motion as well as lateral-directional motion.

All of the above observations will be used for designing the automatic flight control system (AFCS) and stability augmentation system (SAS) in the next stage of the airship development.

Acknowledgement

The authors would like to acknowledge that this work was mainly supported by Korea Ministry of Commerce, Industry and Energy (MOCIE).

References

1. Khoury, G.A. and Gillett, J.D., 1999, *Airship Technology*, Cambridge University Press, Cambridge, UK.

2. Freeman, H.B, 1932, "Force Measurements on a 1/40-Scale Model of the U.S. Airship, AKRON", *NACA-TR No. 432.*

3. Rizzo, F., 1924, "A Study of Static Stability of Airships", *NASA-TN No. 204.*

4. Ho-Nam, Ok, 2001, "Aerodynamic Design of a 50m Class Airhsip and Prediction of its Aerosynamic Characteristics", *KARI-AD-TM-2001-006.*

5. Gomes, S.B.V, 1990, "An Investigation of the Flight Dynamics of Airship with Application to the YEZ-2A", *College of Aeronautics Ph.D. thesis*, Cranfield Institute of Technology.

6. Greensite, 1970, *Analysis and Design of Space Vehicle Flight Control Systems*, Spartan Books.

7. Nelson, R.C, 1990, *Flight Stability and Automatic Control*, McGraw-Hill Book Company, New York.

8. DeLaurier, J. and Schenck, D., 1979, "Airship Dynamic Stability", *AIAA Paper 79-1591.*